ACS OMEGA

Open Access

http://pubs.acs.org/journal/acsodf

Article

Comparison of Toughening Effects of Various Additives on Phenolic Foam

P. Reghunadh Sarika, Paul Nancarrow,* and Taleb Ibrahim

Cite This: *ACS Omega* 2024, 9, 4695−4704

Read Online

ACCESS | Metrics & More | Article Recommendations | Supporting Information

ABSTRACT: Phenolic foams (PFs) are considered excellent insulation materials owing to their flame retardancy and low thermal conductivity. However, their mechanical properties often lag behind those of other polymeric insulation materials. To fully exploit their properties and broaden end-use applications, the mechanical properties of PFs must be enhanced. In this study, various modifications were introduced into the PF matrix with the aim of enhancing its properties. The toughening effects of four additives: urea (U), nano clay (NC), sodium silicate (SS), and lignin (Li) were studied and compared. Changes that occurred in the density, cell morphology, thermal conductivity, compressive strength, and thermal stability after the addition of these fillers were analyzed. Both compressive strength and thermal stability increased with the inclusion of all additives, and the SS-toughened foam shows the biggest improvement. Li and NC addition resulted in a 34% improvement in compressive strength, while SS and U addition displayed increases of 52 and 11%, respectively. SS-toughened PF shows greater improvements in all of the important properties compared with those of the other toughened foams. Several PFs were prepared by changing the SS concentration to optimize the formulation, which yielded improvements in properties. The effects of SS concentration on density, thermal conductivity, and compressive strength were studied. The formulation with 0.37% sodium silicate concentration (PF-SS1) shows a 15% improvement in mechanical properties.

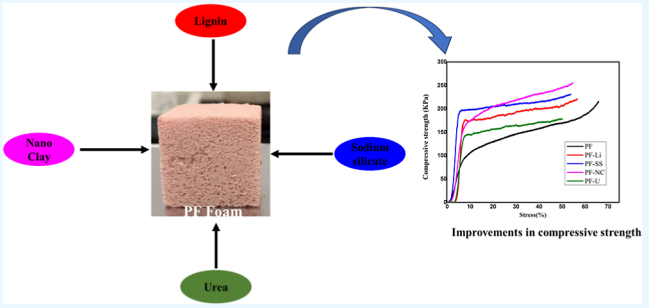

1. INTRODUCTION

Phenolic foams (PFs) have been mainly used as insulators in buildings due to their high thermal stability, low smoke density, and flame retardance.[1,2] However, their low mechanical strength compared to that of other foams, such as polystyrene, polyurethane, and melamine, limits their range of applications.[3] Several efforts have been made over the years to improve these properties, either through the incorporation of additives or by chemical modification of the phenolic resin matrix.[4] These modifications usually increase the compressive strength, flexural strength, and flame retardancy to various extents. The percentage of improvement in each property depends on the type, concentration, and size of the various fillers/additives and chemical modifiers employed in the formulation.

Some of the fillers that had already been used as reinforcing agents in PFs include cellulose fibers,[5] lignin (Li) particles,[6] wood flour,[7] hollow glass beads,[8] multiwalled carbon nanotubes,[9,10] nano silica, and titanium nitride nanoparticles. In the fiber reinforcement method, the main influential parameters are its stiffness, concentration, and compatibility with the resin matrix.[11] In the case of nanoparticle-toughened foams, their size, shape, surface properties, and dispersion efficiency determine the enhancements in thermal stability, flame retardancy, and compressive strength. Chemical modification of the PF matrix is achieved through partial or complete substitution of either phenol or formaldehyde reagents during resin preparation. Biomass-derived materials, such as Li, cardanol, and tannin, have been studied as phenol substitutes during the PF preparation.[12] Through this modification method, long and flexible chains are introduced into the resin matrix, which can improve the mechanical properties.

Li is a biomass-derived material that has been widely used as a PF-toughening additive, both as a reinforcing agent and as a substitute for phenol in the chemical modification toughening method. In both toughening approaches, the concentration of Li plays a critical role in enhancing the mechanical strength. However, during particle reinforcing, a very high concentration of Li particles increases the viscosity of the resin, resulting in problems with mixing and foam expansion. This may cause a significant increase in density and, thus, an increase in thermal conductivity, resulting in diminished insulation properties of the foam. Xu and co-workers found that the density of Li-substituted foam rises from 43 to 108 kg/m^3 with 50% Li-

Received: October 11, 2023
Revised: January 4, 2024
Accepted: January 10, 2024
Published: January 19, 2024

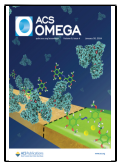

substituted resin. The high viscosity of the 50% Li-substituted resin restricts bubble formation, leading to an uncontrolled increase in the density of the foam. The 50% Li-substituted PF foam was found to exhibit a compressive strength of 0.405 MPa, while 30% substituted foam had a compressive strength of 0.152 MPa.[13]

Del Saz-Orozco et al.[14] extensively studied the reinforcing capability of Li nanoparticles on PF. Toughening with Li nanoparticles resulted in an increase in the compressive strength by 174%. In addition to their reinforcing ability, Li nanoparticles were also found to act as nucleating agents, facilitating the initiation of bubbles and thus enabling a reduction in the blowing agent concentration.

Clay is another important filler used to enhance the mechanical properties of PF. Different types of clay, including kaolin, mineral clay, montmorillonite, cloisite, and nanoclay (NC), have been used as fillers and toughening agents. Wei et al.[15] modified PF with montmorillonite/carbon fibers, and the reinforcement resulted in a 35−40% increase in the compressive strength. Sometimes clay has been used along with fibers to impart improvements in several properties including compressive strength, thermal stability, flame retardancy, brittleness, and pulverization properties simultaneously.[16] Hu et al. used nanocrystals along with glass fibers to enhance the mechanical and thermal properties of phenol−urea−formaldehyde foam. Both additives show synergistic improvements in the compression strength, thermal stability, and flame retardancy of the foam.[17]

The toughening ability of sodium silicate (SS) has also been analyzed in this work. SS is usually used as an alternative blowing agent[18−20] or a precursor for silica production.[21] Phenol−urea−formaldehyde resin has been extensively studied for various applications such as adhesive and foam making.[22,23] Urea (U) was added to the resin to reduce the residual formaldehyde content. In this report, U has been added to the phenol−formaldehyde as a toughening agent, instead of using it as a modifier during the resin formation, and its effect on the properties has been studied.

In this work, we compare the toughening effects of various fillers, such as Li, SS, U, and NC, into PF. Pure and toughened PFs were prepared, and their various properties including apparent density, thermal conductivity, compressive strength, and thermal stability were evaluated and compared. The filler which shows better improvements in mechanical properties was selected for further studies, and its optimum concentration required for providing the highest enhancement was evaluated.

2. EXPERIMENTAL SECTION

2.1. Materials. Phenol (detached crystal) was purchased from Fisher, UK. Formaldehyde solution (37%), sodium hydroxide, polyethylene glycol 600, and *n*-hexane were obtained from Merck. Methanesulfonic acid (Lutropur MSA) and Agnique CSO-30 were provided by BASF. Agnique CSO 30 is an ethoxylate castor oil, which is mainly used as a nonionic water-soluble emulsifier. Additives used in this work include halloysite NC, Li fiber, U, and SS. Halloysite nanocrystal which was obtained from Sigma-Aldrich (Cas no. 1332-58-7) is also known as Kaolin clay with a chemical formula of $H_4Al_2O_9Si_2{\cdot}2H_2O$. It has a morphology of hollow tubes with size less than 100 nm. Li fiber was supplied by EastChem, China. It is an organic fiber obtained by the chemical treatment of wood. U, also known as carbamide, with the chemical formula CH_4N_2O was obtained from LabChem, USA. SS powder (Code A8005-M) was purchased from AVONCHEM, UK. All the additives were used as-supplied without further purification.

2.2. Methods. *2.2.1. Synthesis of Phenolic Resin.* The phenolic resin was synthesized from phenol (P) and formaldehyde (F) with a F/P ratio of 1.5. The synthesis was carried out in a 1 L, three-necked round-bottomed (RB) flask equipped with a thermometer, reflux condenser, and a dropping funnel. The reactor was heated in an oil bath equipped with a magnetic stirrer. Phenol (1 mol) was charged into the RB flask and melted at 40−45 °C. Sodium hydroxide aqueous solution (15 mL, 50%, w/v) was added to the reaction mixture to adjust the pH to 9 and maintain the reaction for 30 min at the same temperature. 80% of the formaldehyde solution was added dropwise through a dropping funnel while the temperature was increased to 60 °C, and the mixture was reacted for 1 h at the same temperature. After 1 h, 5 mL of NaOH was added, and the temperature was increased to 85 °C. When the temperature was rising and reached 70 °C, the remaining formaldehyde was added, and the mixture reacted for 2.5 h at 85 °C. After the reaction, the resin was cooled down to 50−60 °C and distilled to remove the water.

2.2.2. Preparation of Standard and Toughened PF. Standard PF and toughened foams were prepared by the same procedure. The required amounts of synthesized resin, polyethylene glycol, and Agnique CSO 30 were taken in a beaker and mixed with a hand blender for 2−3 min. Hexane was added to this mixture and mixed for a minute. Next, methanesulfonic acid was added and mixed for another minute, and the foaming mixture was immediately poured into a closed-type mold and cured at 80 °C for 1 hour. Postcuring was performed at 60 °C for 2h.

Toughened PFs were prepared by the same procedure with the addition of various additives during the stage of mixing the resin with the blowing agent. Prepared formulations are listed in Table 1. PFs toughened with Li, SS, NC, and U are denoted as PF-Li, PF-SS, PF-NC, and PF-U, respectively.

Table 1. Formulations of Standard PF and Toughened Foams

	PF	PF-Li	PF-SS	PF-NC	PF-U
resin viscosity (mPa·s)	3200	3200	3200	3200	3200
resin (g)	50	50	50	50	50
agnique 30 (g)	4	4	4	4	4
PEG (g)	3	3	3	3	3
hexane (mL)	7	7	7	7	7
L-MSA (mL)	4	4	4	4	4
lignin (g)	0	0.25	0	0	0
sodium silicate (g)	0	0	0.25	0	0
nano clay (g)	0	0	0	0.25	0
urea (g)	0	0	0	0	0.25

Several foams were prepared by varying the concentration of SS, and their properties were compared. Phenol formaldehyde resin with a viscosity of 5580 mPa·s was used to formulate the PF-SS foams. Foams were denoted as PF-SS1, PF-SS2, PF-SS3, and PF-SS4. Table 5 shows the various formulations of SS-toughened foams.

2.3. Characterization. The synthesized phenolic resin and prepared foams were characterized by various methods. Resin

https://doi.org/10.1021/acsomega.3c07967
ACS Omega 2024, 9, 4695−4704

Table 2. Properties of Standard PF and Toughened Foams

sample	density (kg/m^3)	thermal conductivity (W/mK)	mean cell size (μm)	mean cell wall thickness (μm)	compressive strength (KPa)
PF	65.28 ± 1.2	0.037 ± 0.0005	60.63 ± 22	16.37 ± 8	130 ± 3.6
PF-Li	66.10 ± 2.4	0.036 ± 0.0005	87.51 ± 45	13.39 ± 9	174 ± 0.2
PF-SS	63.95 ± 1.1	0.035 ± 0.0005	52.72 ± 18	19.97 ± 5	198 ± 1.4
PF-NC	72.60 ± 1.3	0.038 ± 0.0005	52.30 ± 22	16.15 ± 5	175 ± 1.8
PF-U	62.59 ± 4.5	0.036 ± 0.0005	58.07 ± 19	14.95 ± 4	144 ± 2.5

viscosity was measured using an NDJ-8S Rotational Viscometer (Shanghai, China) at room temperature (25 °C). The solid content of the resin was analyzed according to ASTM standard D4426-01.

2.3.1. Apparent Density. The apparent densities of all of the foam samples were measured as per the ASTM D1622 standard. Results were reported as an average of three samples each with a size of 30 × 30 × 30 mm^3.

2.3.2. Thermal Conductivity. The thermal conductivity of the foams was analyzed on a TCi thermal conductivity analyzer (C-Therm, Canada) using a foam sample size of 30 × 30 × 30 mm^3 at room temperature (25 °C). An average of three samples was reported.

2.3.3. Scanning Electron Microscopy. The morphology of standard PF and various toughened foams was recorded using a scanning electron microscope (TESCAN VEGA 3) with an accelerating voltage of 20 kV. Foam samples were first sputter-coated with a gold conductive layer and then visualized using scanning electron microscopy (SEM). Mean cell size, cell wall thickness, and cell size distributions of the foams were calculated from SEM images using ImageJ software. The cell sizes of at least 100 cells were obtained from SEM images using ImageJ software, and the cell size distribution histograms were plotted based on the obtained cell sizes.

2.3.4. Thermogravimetry. The thermal stability of the foam samples was analyzed using thermogravimetric analysis (TGA) (PerkinElmer, STA 6000) at a scan rate of 10 °C min^{-1} under nitrogen (20 mL/min) from 30 to 850 °C.

2.3.5. Compressive Strength. Foam compressive strength was measured using a universal testing machine (Instron 5580) at room temperature, according to ASTM D1621. At least three foam samples with size 30 × 30 × 30 mm^3 were tested.

3. RESULTS AND DISCUSSION

In this work, two resins having moderate viscosities of 3200 and 5580 mPa·s, respectively, were used for foam making. Resin viscosity plays an important role in the foaming process as it determines the density and other properties of the foam. The highly viscous resin could result in a dense foam having very high thermal conductivity, while a foam from low viscous resin has diminished mechanical strength. To prepare the formulations for comparing the toughening effect of various additives, resin with lower viscosity (3200 mPa•s) was used for ensuring the uniform distribution of additives in the resin matrix. The resin (3200 mPa·s) has a solid content of 72.3%.

Foams were prepared by simple mixing of surfactants, fillers, foaming agents, and curing agents for a few minutes, and curing was done at 80 °C in a closed mold. Fillers used in these experiments were nanocrystal, U, Li, and SS. Optimized formulations are listed in Table 1. Standard PF was prepared without any fillers, and the toughened foams were prepared by adding equal masses of various fillers into the phenolic resin foamable mixture.

3.1. Density. Densities of PF and toughened foams are listed in Table 2. Density plays an important role in determining the physical and mechanical properties of a foam as it is closely related to its cell morphology. Foam density depends on the foam expansion rate, which can be easily modulated by adjusting the blowing agent, or the nucleating agent concentration.[24] Toughening agents sometimes act as nucleating agents that, along with blowing agents and operating conditions, influence the foam expansion process and, hence, the density. Fillers added to the resin matrix impart toughening by altering the cell structure and morphology. The toughening agents used in this work have various impacts on the density of the foam. Changes in the density of PF with the addition of additives, namely, Li, SS, NC, and U, are shown in Figure 1.

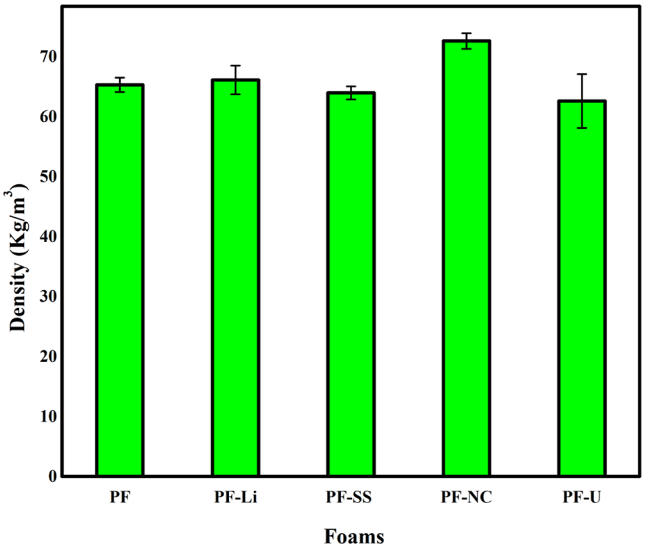

Figure 1. Density of standard PF and toughed PFs.

Density increased with the addition of Li and NC, whereas it reduced after the addition of SS and U. Li and NC increase the viscosity of the foaming resin during mixing, which reduces the foam expansion rate, leading to a slight increase in the corresponding foam density. According to Yang et al., the nucleator's diameter and bulk density are responsible for the changes in viscosity of the foaming resin.[25] Distribution of Li and nanocrystal fillers in the resin matrix was not uniform due to the increase in viscosity, which results in an increase in the density of the resulting foam. Li-toughened foams have a density of 66.10 ± 2.4 kg/m^3, while the PF-NC has a density of 72.60 ± 1.3 kg/m^3. SS- and U-toughened foams show a decrease in density. SS has been used as a blowing agent in ceramic foam making. The addition of U and SS induces more bubble formation, and the foam expansion becomes easy; thereby, the resulting foam has low density.

https://doi.org/10.1021/acsomega.3c07967
ACS Omega 2024, 9, 4695−4704

3.2. Thermal Conductivity. PFs are expected to have a very low thermal conductivity for their application as insulation materials.[26] The insulation efficiency of the foam is inversely proportional to its thermal conductivity. Low thermal conductivity provides a high resistance to heat transfer, which helps reduce energy loss, and thus, a lower thickness of the material is needed. Hence, foam with lower thermal conductivity is preferred to save energy, cost, and space. At the macroscopic level, the thermal conductivity of a foam is the cumulative result of conduction across the gas phase, conduction through the solid matrix, convection within the cells, and radiation interchanging in participating media. At the microscopic level, it depends on the foam morphology characteristics such as cell size,[4] cell density, proportion of open versus closed cells, and cell size distribution of foam.[27] The foam morphology and the nature of the gas inside the cells are crucial in determining the thermal conductivity of a foam.[28] There are several studies on the effect of various parameters, such as density, cell size, cell size distribution, and porosity on the thermal conductivity of porous materials.[29,30] Soloveva et al. studied the effect of cell size and type on the thermal conductivity of polyurethane foam.[31] Foams with uniform, small, and closed cells show low thermal conductivity. In order to reduce the thermal conductivity, the cell morphology must be optimized. Fillers, nanoparticles, or other additives added to the foam to improve their properties can influence the cell morphology and, thereby, the thermal conductivity. In addition to the morphology, foam density also influences the thermal conductivity as the main portion of heat transfer occurs via conduction through the solid. Highly dense foam has high thermal conductivity owing to the low porosity and low gas content in small cells. As density decreases, thermal conductivity also decreases until it reaches a limit below which the structural integrity of the cells is compromised, resulting in a higher proportion of open cells.

The thermal conductivities of the standard and toughed PF are shown in Table 2. All of the toughened foams, except PF-NC, show lower thermal conductivity than that of the standard PF. In this work, the standard PF exhibits a thermal conductivity of 0.037 W/mK, which was reduced to 0.036 W/mK after toughening with Li and to 0.035 W/mK with SS. NC addition was found to increase the density of the foam to a considerable extent and also its thermal conductivity. Each additive has a unique influence on the morphology of the PF, which results in an increase or decrease in the thermal conductivity. In foams made from Li-substituted resin, the presence of Li does not have any significant impact on its thermal conductivity.[28] Li particle addition into standard PF slightly increases the density and changes the cell morphology including cell size and cell size distribution. Usually, foams having high density have a higher volume ratio of solid matrix to gas cells and, therefore, exhibit high thermal conductivity as the conduction through the solid matrix contributes more toward the thermal conductivity. However, a slight decrease in thermal conductivity is observed in Li-toughened PF foam, even though its density has increased. This unusual characteristic may be due to the uneven distribution of Li in the resin matrix and the resulting irregular foam expansion. The broad cell size distribution in PF-Li also confirms the nonuniformity of the cell structure. The gas trapped in the large cells contributes more to the overall thermal conductivity of PF-Li, causing a reduction in thermal conductivity. In SS-modified foam, density has decreased, and the cells are small and uniform compared to that in the pure and other toughened foams. It is thought that SS could facilitate the formation of a thin layer within the closed cells of the foam and retain more of the blowing agent inside the cell, thus reducing the thermal conductivity.[32] Hence, it has the lowest conductivity among all the toughened foams, and it is due to the combined effect of low density, small cell size, and uniform cell structure. Among all the toughened foams, PF-NC shows the highest thermal conductivity of 0.038 (W/mK). In highly dense foam, conduction through the solid part is more, which also helps increase the thermal conductivity. In PF-NC, high density and small cells contribute to an increase in thermal conductivity. The foam with added U displays the lowest density compared with that of the other toughened foams and standard PF foam. However, while PF-U has a lower density than PF-SS, it has a slightly higher thermal conductivity due to the broad size distribution of cells.

3.3. Morphology. SEM was used to analyze the cell structure of standard PF and toughened foams, and the images are shown in Figure 2. The standard PF contains nonuniform open and closed cells with spherical and elliptical morphology. This anisotropy in the PF foam is due to the free expansion of the foaming resin to the top surface along the molding wall, whereas, in toughened foams, fillers control the expansion process by imparting changes in viscosity and bubble formation. Cell size distributions of standard and toughened foams are listed in Figure 3. In PF foams (Figure 2A1,A2), the cell size distributions are in the range of 21−152 μm with a mean size of 60.63 μm. Around 45% of cell size distributions of PF foam are concentrated in the 20−40 μm region. Cell walls of the standard PF have a thickness of 16.37 μm, as shown in Table 2. Cell morphology changes from elliptical to honeycomb shape in Li-toughened foam (PF-Li, Figure 2B1,B2), and the cells have larger diameters compared to those of the pure PF foam. The large and closed cells decrease the thermal conductivity of PF-Li to 0.036 W/mK. Its cell size ranges from 23.57 to 213.86 μm with an average size of 87.51 μm. The increase in cell size and the broad cell size distribution are due to the agglomeration of Li particles in the cell matrix. The nonuniform distribution of Li leads to an uneven expansion of resin, resulting in broad cell distribution with 34% of cells with size up to 80 μm.

SS-toughened foams (PF-SS, Figure 2C1,C2) have a uniform and small spherical cell in their structure. SS could act as a nucleating agent for bubble formation of the foaming agent hexane. Resin mixing and foam expansion become easy and help form a uniform structure. The cell size distribution becomes narrow with 25% of the cells falling in the size range of 40−50 μm. The cell wall thickness increased from 16.5 to 19.8 μm with SS modification. This uniform, small cells contribute to a very low thermal conductivity. The thick cell wall can bear the load for a longer period than thin cell walls, meaning PF-SS has a high compressive strength.

NC-reinforced foam (PF-NC, Figure 2D1,D2) also has spherical and small cells with wall thickness around 11 μm. It has a nonuniform cell structure with cell size ranging from 13 to 115 μm. High density and the nonuniform small cells result in the higher thermal conductivity of NC-toughened foam. U-toughened foams (PF-U, Figure 2E1,E2) also have cells with size ranging from 19 to 116 μm with an average size of 58 μm and cell wall thickness of 15 μm. Addition of U decreases the viscosity of the foaming mixture significantly, which causes the fast expansion of the foaming mixture. The cell size

https://doi.org/10.1021/acsomega.3c07967
ACS Omega 2024, 9, 4695−4704

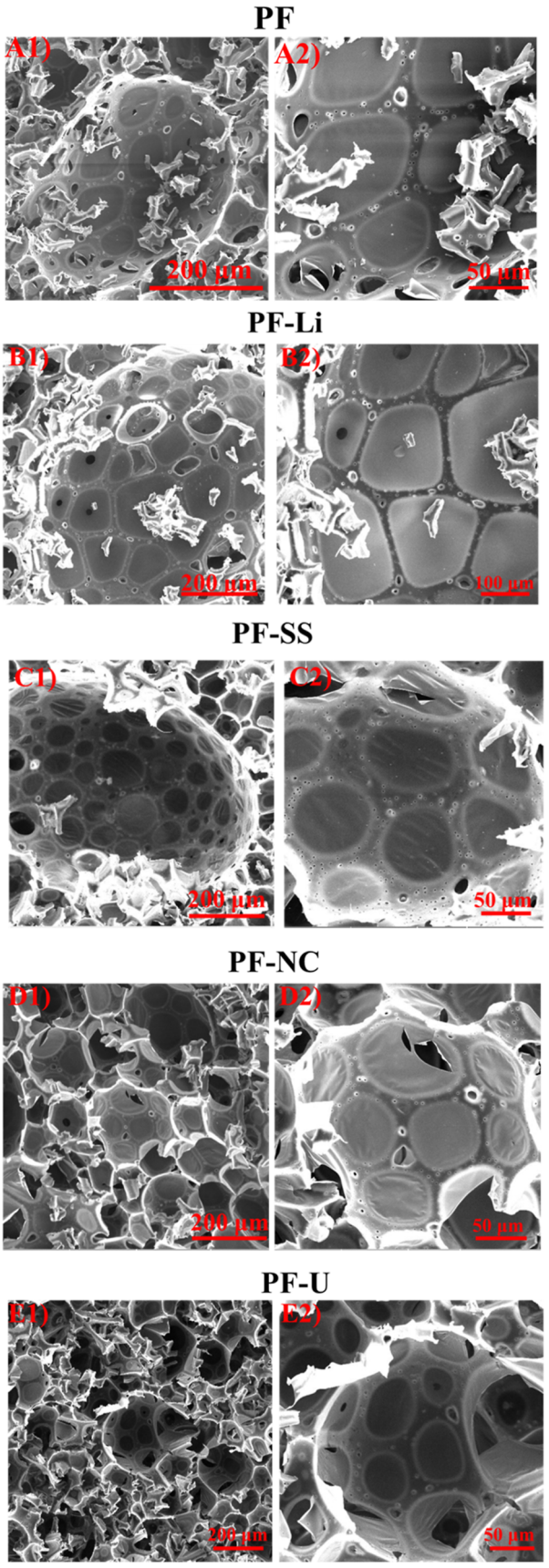

Figure 2. High- and low-resolution SEM images of PF (A1,A2), PF-Li (B1,B2), PF-SS (C1,C2), PF-NC (D1,D2), and PF-U (E1,E2) foam.

distribution becomes broad due to the easy expansion of the foaming mixture. This free expansion leads to the bursting of cells, resulting in a large proportion of open cells. The low compressive strength is due to the presence of open cells in its structure.

3.4. Thermal Stability. Thermal stability of all foams was analyzed via TGA. The TGA and differential thermogravimetry (DTG) graphs of pure and toughened foams are shown in Figure 4A,B, respectively. Thermal stability of the PF increased after toughening, and the rate of toughening was found to vary depending on the fillers used. Residual weight percentage at different temperatures for the various foams is listed in Table 3. PFs usually have three degradation steps: below 200 °C, second step between 200 and 400 °C, and the final stage in the range of 400−800 °C. The first degradation occurs below 200 °C, which corresponds to the volatilization of water, unreacted phenol, formaldehyde, foaming agent, and any other low-molecular-weight substances present in the cured foam. The second stage between 200 and 400 °C results from the degradation of surfactants, curing agents, and diphenyl ether bond condensation−dehydration. The third, occurring between 400 and 800 °C, corresponds to the breakage of the ring structure and the long chains. Both PF and toughened foams show similar TGA and DTG patterns with a different T_{max} at various degradation stages. T_{max} values obtained from the DTG curve at different stages are listed in Table 3. PF and NC-toughened foams show similar behavior up to 700 °C, and PF-NC exhibits a high residual weight percentage after that. The second step of the curve corresponds to the region between 200 and 400 °C and denotes the decomposition of the weak polymer chains in the foam. The residual weights of PF and PF-NC are the same during this stage, while the other toughened foams have a high residual weight. In the third stage, above 500 °C, carbonaceous material is produced, and all the toughened foams show similar TGA patterns; their residual weights are higher than those of pure PF. The residual weight values of all foams at different temperature are shown in Table 3, and it is higher for all modified foams compared with that of PF at 400, 600, and 800 °C. Li-, U-, and SS-toughened foams show the same TGA pattern with slight changes in residual weight percentage at 800 °C. SS- and U-toughened foams show better stability at 400 and 800 °C than that of other foams. Weight loss of 25% was reached at temperatures of 445 °C for PF, 452 °C for PF-L, 457 °C for PF-SS, 440 °C for PF-NC, and 455 °C for PF-U.

3.5. Compressive Strength. As mentioned previously, the main drawback of PF is its low mechanical strength compared to that of other polymeric insulation foams. Improving the compressive strength is essential for widening its application areas. Compressive strength of standard PF and toughened foams was measured as per standard ASTM D1621; the results are listed in Table 4, and the stress−strain curves are shown in Figure 5.

Standard PF has a strength of 130 ± 3.6 KPa, which has been increased after toughening with various additives. The increase in mechanical strength resulting from the incorporation of particle toughening agents is considered to be due to the effect of such additives on cell morphology. Particles can act as nucleating agents, and their presence increases bubble formation, which eventually leads to an increase in cell density. This also results in a uniform cell morphology with small cells. Though particles could improve the cell morphology, careful control of their concentration is highly essential as it can

https://doi.org/10.1021/acsomega.3c07967
ACS Omega 2024, 9, 4695−4704

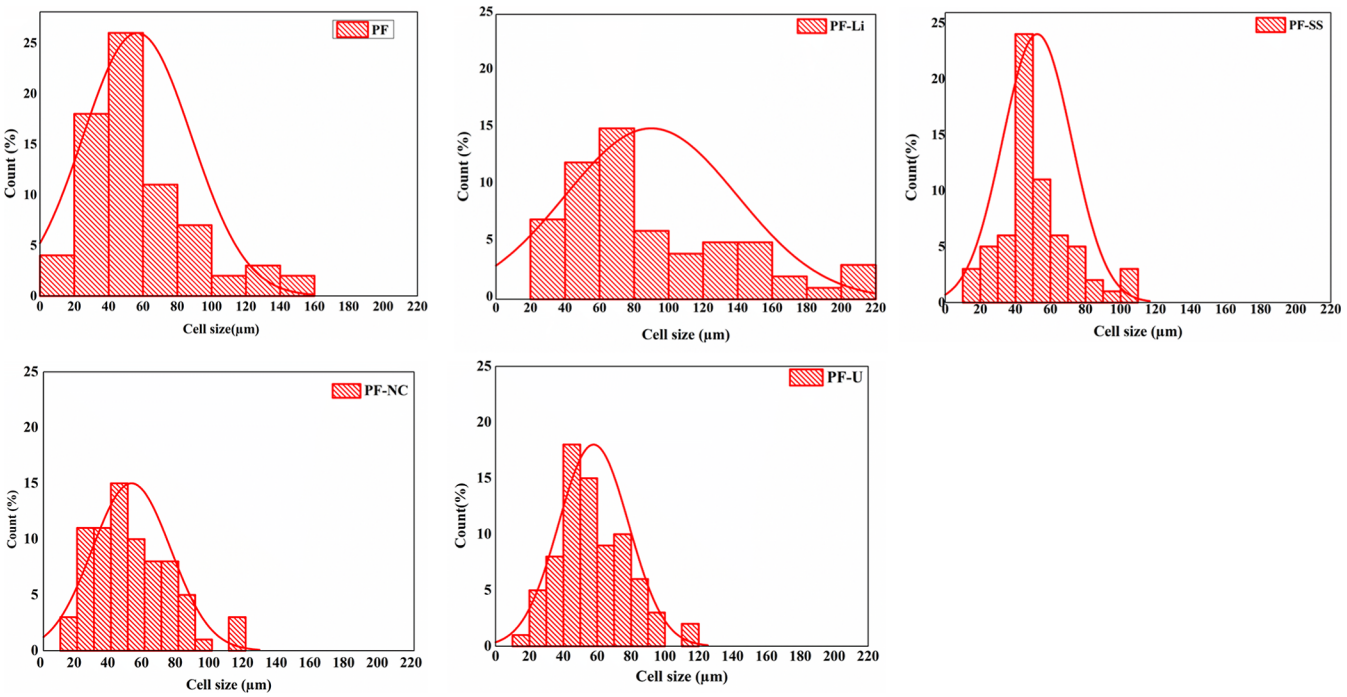

Figure 3. Cell size distribution of standard and toughened PF foams.

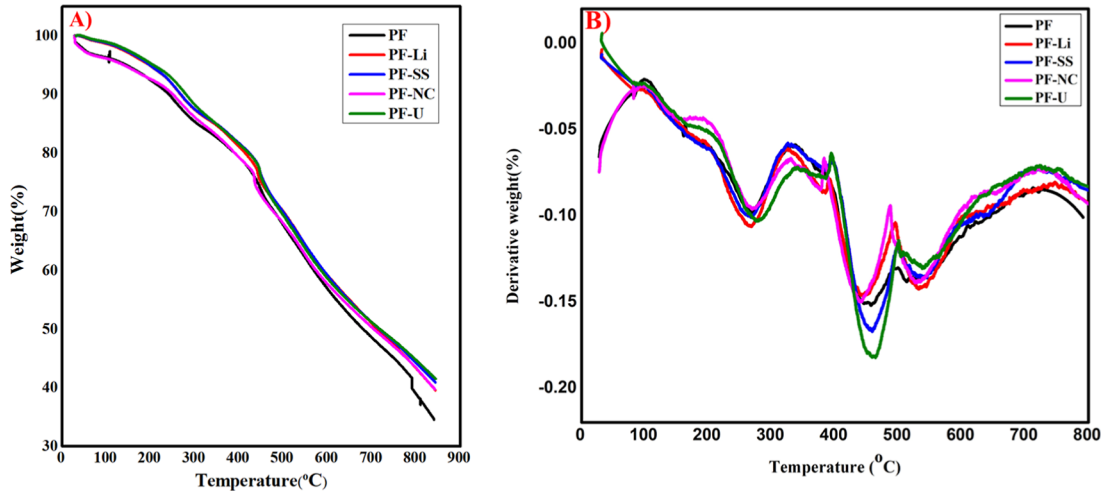

Figure 4. TGA (A) and DTG (B) thermograms of pure and toughened foams.

Table 3. Residual Weight Percentage of Pure and Toughened Foams at Various Temperatures[a]

	residual weight %			T_{max} at 200−400 °C	T_{max} at 400−800 °C
	400 °C	600 °C	800 °C		
PF	79.05	56.43	40.83	268	453
PF-Li	80.87	58.86	43.38	269	442
PF-SS	81.53	58.52	44.06	267	458
PF-NC	78.83	56.82	43.38	270	439
PF-U	81.14	58.52	44.44	281	461

[a] T_{max}—maximum degradation temperature, Residual weight—mass left in the sample.

Table 4. Cell Structure Details and Compressive Strength of Standard and Toughened PFs

	cell size (μm)	cell wall thickness (μm)	compressive strength (KPa)
PF	60.63 ± 22	16.37 ± 8	130 ± 3.6
PF-Li	87.51 ± 45	13.39 ± 9	174 ± 0.2
PF-SS	52.72 ± 18	19.97 ± 5	198 ± 1.4
PF-NC	52.3 ± 22	16.15 ± 5	175 ± 1.8
PF-U	58.07 ± 19	14.95 ± 4	144 ± 2.5

increase the viscosity of the foaming matrix and thereby the density.[33]

Each additive shows a unique effect on the compressive strength based on its influence on foam morphology and density. Foams toughened with SS have the highest strength compared to that of those of the other synthesized foams. Usually, the compressive strength is directly proportional to the density of the foam. But here, a low-density foam (PF-SS) shows the highest strength, which results from its uniform cell

https://doi.org/10.1021/acsomega.3c07967
ACS Omega 2024, 9, 4695−4704

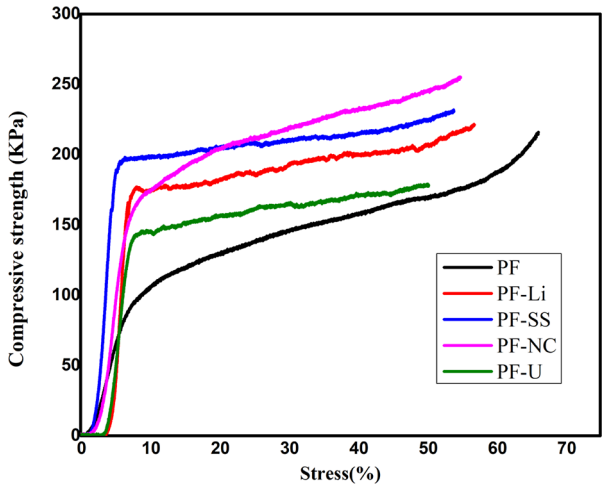

Figure 5. Stress−strain curves of standard PF and toughened PFs.

structure with small cells and thick cell walls. This is possibly due to SS acting as a nucleating agent,[19] enhancing bubble formation and thereby increasing the cell density and reducing cell size. PF-SS foams have a mean cell wall thickness of 19.97 ± 5 μm, the highest among the other toughened foams and standard PF. Cells with thick cell walls could resist the cracking of cells under applied load for a longer period, which implies higher mechanical strength. In addition to that, the interaction between Si−O bonds in the silicate and the phenolic −OH groups of the resin improves the mechanical properties by enhancing chain flexibility. The long chains exhibited resistance to cell rupture under applied load by bearing the destruction energy, increasing the threshold of induced cracks and reducing the propagation rate of cracks.[34] Both NC- (PF-NC) and Li- (PF-Li) reinforced foams show 34% increased compressive strength even though significant differences were observed in their densities. This is attributed to the differences in their cell morphology as shown in Figure 2. In PF-Li foams, the high compressive strength is attributed to its high density and the honeycomb-like morphology of the cells. The honeycomb-like cells can disperse the external stress more effectively than circular cells.[34] Li is a carbohydrate polymer that contains a number of hydroxyl groups in its structure. These hydroxyl groups can participate in the condensation reaction of phenolic resin by reacting with the hydroxyl groups on them and forming hydroxymethyl groups in the resin. Thus, Li molecules could be incorporated into the structure of the phenolic resin during the foaming process. The introduction of Li molecules in the resin structure will impart flexibility to the chains, and hence, it can withstand the applied stress/load for a longer time even though the PF-Li foams have large size and thin cell walls. Xu et al.[35] added montmorillonite to increase the flame retardancy of the bio-oil substituted PF. In addition to that, their compressive strength and limiting oxygen index were also improved by 31% and 33%, respectively. Cloisite-10A-clay-nanoparticle-infused PF foam shows 80% increase in compressive strength.[33] Li has been extensively used in PFs as a biobased substitute[36] or as a filler[7] to improve the properties of the foam. Del Saz-Orozco et al.[14] found that the Li nanoparticle reinforcement increases the compressive strength of PF by 174%. In NC-toughened foams, their high density, small cell size, and thick cell walls contribute to the observed rise in mechanical strength. Addition of U also enhanced the compressive strength, albeit to a lesser extent, compared to that by other additives. U addition decreases the viscosity of the foamable resin mixture, which facilitates mixing and helps expand the foam quickly. Though the density of U-modified PF is less than that of the standard PF, it shows higher compressive strength due to the uniform cell morphology. U is usually added to PF to reduce the amount of unreacted formaldehyde and thus to reduce the toxicity of the foam. It has also been used to toughen the foam.[37]

Of the additives compared in this study, it is clear that SS has the greatest impact on toughening the PF. Hence, it has significant potential for improving the properties of PF. Optimization studies were performed to finalize the appropriate concentration of SS required to provide the maximum toughening effect. SS-toughened foams with slight changes in the concentration of poly(ethylene glycol) (PEG) and MSA in the foam formulation were made to optimize the properties of the resulting foams compared to those formulations listed in Table 1. Various PF-SS foams were prepared by changing the concentration of SS, and the effect of concentration of SS on the properties of the foams were evaluated. Table 5 represents the PF-SS foam formulations with varied percentages of SS.

Table 5. Formulations of PF-SS Foams with Various Percentages of Sodium Silicate

	PF1	PF-SS1	PF-SS2	PF-SS3	PF-SS4
resin (g)	50	50	50	50	50
agnique 30 (g)	4	4	4	4	4
PEG (g)	3.2	3.2	3.2	3.2	3.2
hexane (mL)	7	7	7	7	7
L-MSA (mL)	4.2	4.2	4.2	4.2	4.2
sodium silicate (g)	0	0.25	0.35	0.4	0.5

Properties of the SS-toughened foams were analyzed and are listed in Table 6, and the effect of SS concentration on density,

Table 6. Properties of PF and SS-Toughened Foams

	density (kg/m^3)	thermal conductivity (W/mK)	comp. strength (kPa)
PF1	62 ± 5	0.036 ± 0.0005	177.5 ± 8
PF-SS1	61 ± 2	0.035 ± 0.0005	204.5 ± 10
PF-SS2	56 ± 2	0.035 ± 0.0005	119.8 ± 5
PF-SS3	54 ± 3	0.035 ± 0.0005	105.4 ± 2

thermal conductivity, morphology, and compressive strength were evaluated. Figure 6 shows the changes in the density of PF-SS foams with respect to the SS concentration. The density of PF decreases with the addition of SS. As explained earlier, SS can act as a nucleating agent as well as a foaming agent. With an increase in concentration, the number of bubbles formed increases, which favors uniform mixing between the foaming agent, resin, and other agents in the resin matrix. The foam expansion rate increases compared to that of the PF1 foams and the density decreased with increase in the SS concentration. After a saturation point, the increase in SS concentration results in agglomeration and nonuniform distribution of reagents in the foaming resin mixture. Hence, in PF-SS4, the high concentration of SS leads to a turbulent expansion of the foaming mixture and a foam with an uneven cell structure. Since there is a huge variation in the structure of PF-SS4 foam due to the uncontrolled expansion, their properties were not evaluated, and the foams with higher

https://doi.org/10.1021/acsomega.3c07967
ACS Omega 2024, 9, 4695−4704

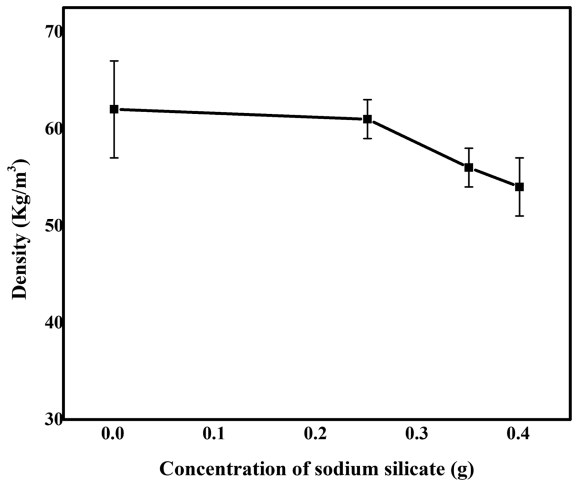

Figure 6. Changes in the density of PF-SS foams with increase in concentration of SS.

concentration of SS (>0.5 g) were also not prepared. Properties of various PF-SS foams are listed in Table 6.

Thermal conductivity of PF reduced with the addition of SS due to the decrease in density and the uniformity of cells in its structure. PF-SS1, PF-SS2, and PF-SS3 foams have the same conductivity due to the low density of the foams. PF-SS4 foams shows similar thermal conductivity as that of PF1 due to the nonuniformity in the cell morphology that originated from the uneven distribution of SS in the resin matrix. Nonuniform and large cells also contribute to the increase in conductivity.

SEM images of PF1, PF-SS1, and PF-SS4 are shown in Figure 7. SS foams, which have high compressive strength, are viewed using SEM to understand their cell structure. PF1 has a mean cell size of 56.51 ± 22 μm and cell wall thickness of 15.44 ± 5 μm.

The cell size increased after the addition of SS due to the effortless expansion of the resin mixture. The mean cell size and cell wall thickness of the three foams are shown in Table 7. In PF-SS1 and PF-SS4 foams, the cell size increased to 70.16 ± 33 and 98.59 ± 53 μm, respectively, with the addition of SS. The mean cell size is higher in PF-SS4 among all the SS-toughened foams owing to the high concentration of SS and resulting uncontrolled expansion.

The thickness of the cell walls of SS PF foams is significantly higher than that of standard PF foams. PF-SS1 foam shows the highest wall thickness among all the foams.

The toughening effect of SS with respect to concentration was evaluated by measuring the compressive strength using a universal testing machine. The stress−stain curves of the various PF-SS foams are shown in Figure 8A. The change in compressive strength as a function of SS concentration is plotted in Figure 8B. The strength of the foam was evaluated based on its ability to withstand the applied load without breaking the cell structure. The nature of the cell structure determines the key properties, including thermal conductivity and compressive strength of the PF. Foams having small and uniform cells with thick cell walls exhibit low thermal conductivity and high compressive strength. In the present work, the effects of the SS concentration on cell morphology and compressive strength of the foam were analyzed.

Table 7. Cell Properties of PF and SS-Toughened Foams

	cell size (μm)	cell wall thickness (μm)
PF1	56.51 ± 22	15.44 ± 5
PF-SS1	70.16 ± 33	30.05 ± 7
PF-SS4	98.59 ± 53	26.85 ± 10

Toughened foams were found to exhibit better mechanical performance than that of the unmodified foams, and the rate of toughening depends on the type and concentration of toughening additives. As shown in Figure 8, the compressive strength of PF-SS foams increases initially with the addition of SS but decreases with higher amounts of SS due to the reduction in density.

In SS-toughened foams, the high compressive strength is due to the thick cell walls. Thick walls could resist cracking for a longer period. The cell wall thickness increased from 15 to 30 μm with the addition of 0.25 g of SS. From the above experiments, it is clear that the PF-SS1 formulation has a high compressive strength and low thermal conductivity at a favorable density. The formulation provides maximum benefits with a minimum number of additives, which is highly recommended for commercial application.

4. CONCLUSIONS

In this work, the toughening effect of various additives/fillers on the properties of PF were studied and compared. The effects of Li, SS, NC, and U on density, thermal conductivity, morphology, and mechanical properties of the foam were analyzed. All of the modified foams exhibit higher compressive strength than that of the standard PF foams, with Li increasing the compressive strength of PF foam by 33%. Its cell structure contains large, honeycomb-like cells with thin cell walls. NC provides a 11% increase in density, which results in increases in both thermal conductivity and compressive strength. Among all the additives, SS-toughened foams have the most promising results as they exhibited a compressive strength increase of 52% while simultaneously displaying decreased thermal conductivity and density compared to those of other foams. It is postulated that the ability of silicate to act as a nucleating

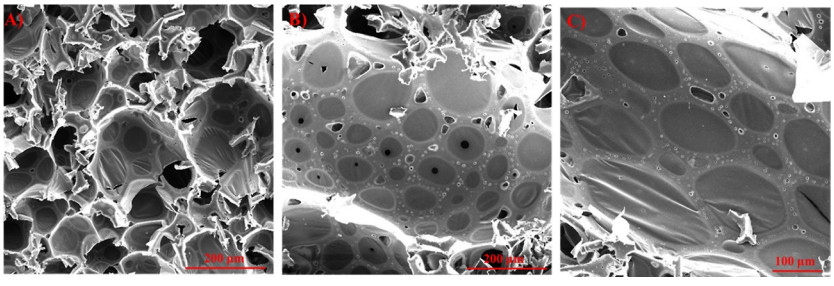

Figure 7. SEM images of PF1 (A), PF-SS1 (B), and PF-SS4 (C). Cell size of the foams increase with increase in SS concentration.

https://doi.org/10.1021/acsomega.3c07967
ACS Omega 2024, 9, 4695−4704

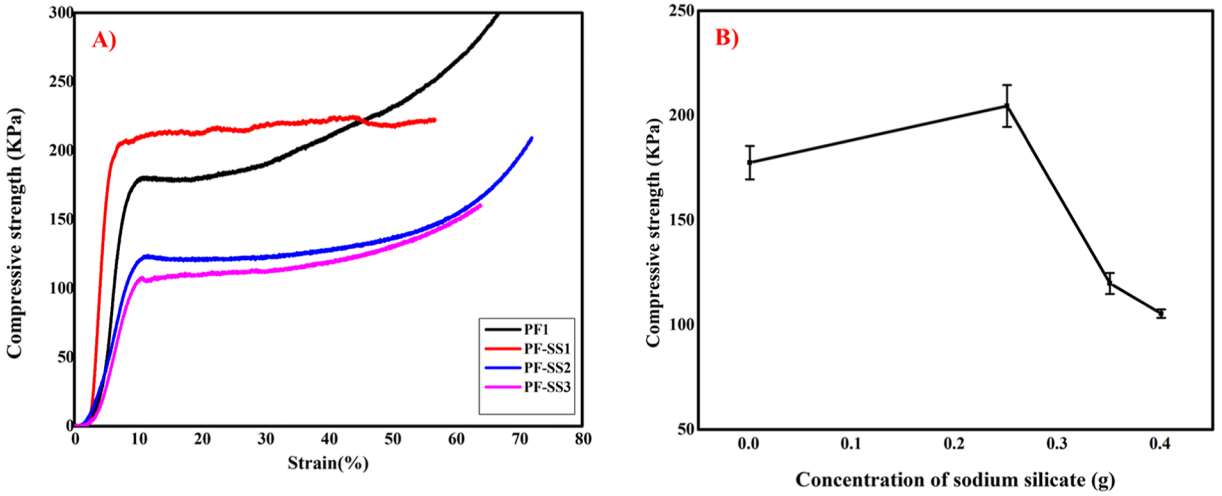

Figure 8. Stress−strain curves of PF-SS foams (A) and changes in compressive strength with respect to the concentration of SS (B).

agent and to establish bonds between the Si═O and hydroxyl groups in the phenolic resin helps facilitate the toughening effect. Although Li has been extensively used as a toughening agent, both as a particle additive and as a chemical substitute for phenol, the addition of SS provides even better properties compared with those with addition of Li. To optimize the minimum concentration of SS for maximum improvements in mechanical properties, various foams were prepared by changing the SS concentration. Density and compressive strength decreased with increases in the concentration of SS. PF-SS1 foam, with the lowest SS concentration studied, shows maximum improvements in properties. These results indicate that SS is a promising toughening agent for commercial PF.

■ ASSOCIATED CONTENT

Supporting Information

The Supporting Information is available free of charge at https://pubs.acs.org/doi/10.1021/acsomega.3c07967.

Energy-dispersive X-ray spectroscopy mapping results for samples PF1, PF-SS1, and PF-SS4 (PDF)

■ AUTHOR INFORMATION

Corresponding Author

Paul Nancarrow − *Department of Chemical & Biological Engineering, American University of Sharjah, Sharjah 26666, United Arab Emirates;* orcid.org/0000-0002-6188-8491; Email: pnancarrow@aus.edu

Authors

P. Reghunadh Sarika − *Department of Chemical & Biological Engineering, American University of Sharjah, Sharjah 26666, United Arab Emirates*

Taleb Ibrahim − *Department of Chemical & Biological Engineering, American University of Sharjah, Sharjah 26666, United Arab Emirates*

Complete contact information is available at: https://pubs.acs.org/10.1021/acsomega.3c07967

Notes

The authors declare no competing financial interest.

■ ACKNOWLEDGMENTS

The authors would like to acknowledge Khansaheb Industries for supporting this work.

■ REFERENCES

(1) Hidalgo, J. P.; Torero, J. L.; Welch, S. Fire Performance of Charring Closed-cell Polymeric Insulation Materials: Polyisocyanurate and Phenolic Foam. *Fire Mater.* **2018**, *42* (4), 358−373.

(2) Zhuang, X. W.; Li, S. H.; Ma, Y. F.; Zhang, W.; Xu, Y. Z.; Wang, C. P.; Chu, F. X. Preparation and Performance Research on Phenolic Insulation Foam Used Low-Temperature Foaming Technology. *Adv. Mater. Res.* **2011**, *250*−*253*, 450−454.

(3) Sandhya, P. K.; Sreekala, M. S.; Thomas, S. Phenolic-Based Foams: State of the Art, New Challenges, and Opportunities. In *Phenolic Based Foams: Preparation, Characterization, and Applications*; Springer, 2022; pp 1−14.

(4) Ge, T.; Tang, K.; Zhang, A. Toughened Phenolic Foams. In *Phenolic Based Foams: Preparation, Characterization, and Applications*; Springer, 2022; pp 81−101.

(5) Del Saz-Orozco, B.; Alonso, M. V.; Oliet, M.; Domínguez, J. C.; Rodriguez, F. Mechanical, Thermal and Morphological Characterization of Cellulose Fiber-Reinforced Phenolic Foams. *Composites, Part B* **2015**, *75*, 367−372.

(6) Carlos Domínguez, J.; Saz-Orozco, B. D.; Oliet, M.; Virginia Alonso, M.; Rodriguez, F. Thermal degradation kinetics of a lignin particle-reinforced phenolic foam. *J. Cell. Plast.* **2021**, *57* (2), 176−192.

(7) Del Saz-Orozco, B.; Alonso, M. V.; Oliet, M.; Domínguez, J. C.; Rojo, E.; Rodriguez, F. Lignin Particle-and Wood Flour-Reinforced Phenolic Foams: Friability, Thermal Stability and Effect of Hygrothermal Aging on Mechanical Properties and Morphology. *Composites, Part B* **2015**, *80*, 154−161.

(8) Zuo, Y. X.; Yao, Z. J.; Zhou, J. T. Mechanical and Thermal Properties of Phenolic Foams Reinforced by Hollow Glass Beads. *Adv. Mater. Res.* **2014**, *988*, 13−22.

(9) Li, Q.; Chen, L.; Li, X.; Zhang, J.; Zhang, X.; Zheng, K.; Fang, F.; Zhou, H.; Tian, X. Effect of Multi-Walled Carbon Nanotubes on Mechanical, Thermal and Electrical Properties of Phenolic Foam via in-Situ Polymerization. *Composites, Part A* **2016**, *82*, 214−225.

(10) Yang, Z.; Yuan, L.; Gu, Y.; Li, M.; Sun, Z.; Zhang, Z. Improvement in Mechanical and Thermal Properties of Phenolic Foam Reinforced with Multiwalled Carbon Nanotubes. *J. Appl. Polym. Sci.* **2013**, *130* (3), 1479−1488.

(11) Mougel, C.; Garnier, T.; Cassagnau, P.; Sintes-Zydowicz, N. Phenolic Foams: A Review of Mechanical Properties, Fire Resistance and New Trends in Phenol Substitution. *Polymer* **2019**, *164*, 86−117.

(12) Sarika, P. R.; Nancarrow, P.; Khansaheb, A.; Ibrahim, T. Progress in Bio-Based Phenolic Foams: Synthesis, Properties, and Applications. *ChemBioEng Rev.* **2021**, *8* (6), 612−632.
(13) Li, B.; Wang, Y.; Mahmood, N.; Yuan, Z.; Schmidt, J.; Xu, C. C. Preparation of Bio-Based Phenol Formaldehyde Foams Using Depolymerized Hydrolysis Lignin. *Ind. Crops Prod.* **2017**, *97*, 409−416.
(14) Del Saz-Orozco, B.; Oliet, M.; Alonso, M. V.; Rojo, E.; Rodríguez, F. Formulation Optimization of Unreinforced and Lignin Nanoparticle-Reinforced Phenolic Foams Using an Analysis of Variance Approach. *Compos. Sci. Technol.* **2012**, *72* (6), 667−674.
(15) Wei, D.; Li, D.; Zhang, L.; Zhao, Z.; Ao, Y. Study on Phenolic Resin Foam Modified by Montmorillonite and Carbon Fibers. *Procedia Eng.* **2012**, *27*, 374−383.
(16) Moni, G.; Silva, S. A. Modification in Phenolic Foams and Properties of Clay Reinforced PF. In *Phenolic Based Foams: Preparation, Characterization, and Applications*; Springer, 2022; pp 209−220.
(17) Hu, X.; Cheng, W.; Nie, W.; Wang, D. Flame Retardant, Thermal, and Mechanical Properties of Glass Fiber/Nanoclay Reinforced Phenol-Urea-Formaldehyde Foam. *Polym. Compos.* **2016**, *37* (8), 2323−2332.
(18) Zhang, D.; Yang, Y.; Sun, X.; Zheng, X. Application and Research Progress of Industrial Waste Residue in the Preparation of Ceramic Foams. In *2020 International Conference on Artificial Intelligence and Electromechanical Automation (AIEA)*; IEEE: Tianjin, China, June 26−28, 2020; pp 865−868.
(19) Chen, X.; Lu, A.; Qu, G. Preparation and Characterization of Foam Ceramics from Red Mud and Fly Ash Using Sodium Silicate as Foaming Agent. *Ceram. Int.* **2013**, *39* (2), 1923−1929.
(20) Uribe, L.; Giraldo, J. D.; Vargas, A. Effect of the Operational Conditions in the Characteristics of Ceramic Foams Obtained from Quartz and Sodium Silicate. *Materials* **2020**, *13* (8), 1806.
(21) Lee, J.; Sohn, K.; Hyeon, T. Low-Cost and Facile Synthesis of Mesocellular Carbon Foams. *Chem. Commun.* **2002**, *2* (22), 2674−2675.
(22) Hu, X. M.; Wang, D. M.; Cheng, W. M.; Zhou, G. Effect of Polyethylene Glycol on the Mechanical Property, Microstructure, Thermal Stability, and Flame Resistance of Phenol-Urea-Formaldehyde Foams. *J. Mater. Sci.* **2014**, *49*, 1556−1565.
(23) Hu, X.; Zhao, Y.; Cheng, W.; Wang, D.; Nie, W. Synthesis and Characterization of Phenol-urea-formaldehyde Foaming Resin Used to Block Air Leakage in Mining. *Polym. Compos.* **2014**, *35* (10), 2056−2066.
(24) Chen, X.; Yu, W.; Ma, L.; Zhou, S.; Liu, X. Mechanical Properties and Thermal Characteristics of Different-Density Phenolic Foams. *J. Therm. Anal. Calorim.* **2021**, *144*, 393−401.
(25) Yang, T.; Dong, Y.; Li, X.; Zhang, J.; Cheng, J. Pore Structure of the Phenolic Porous Material and Its Mechanical Property. *J. Cell. Plast.* **2015**, *51* (4), 401−412.
(26) Ma, Z. Thermal Conductivity of Phenolic Foams. In *Phenolic Based Foams: Preparation, Characterization, and Applications*; Springer, 2022; pp 155−174.
(27) Li, J.; Zhang, A.; Zhang, S.; Gao, Q.; Zhang, W.; Li, J. Larch Tannin-Based Rigid Phenolic Foam with High Compressive Strength, Low Friability, and Low Thermal Conductivity Reinforced by Cork Powder. *Composites, Part B* **2019**, *156*, 368−377.
(28) de Carvalho, G.; Pimenta, J. A.; dos Santos, W. N.; Frollini, E. Phenolic and Lignophenolic Closed Cells Foams: Thermal Conductivity and Other Properties. *Polym. Plast. Technol. Eng.* **2003**, *42* (4), 605−626.
(29) Hasanzadeh, R.; Azdast, T.; Doniavi, A.; Lee, R. E. Multi-Objective Optimization of Heat Transfer Mechanisms of Microcellular Polymeric Foams from Thermal-Insulation Point of View. *Therm. Sci. Eng. Prog.* **2019**, *9*, 21−29.
(30) Zhu, J. Impact of Size Distribution of Cell Model on the Effective Thermal Conductivity of Saturated Porous Media. *Int. J. Thermophys.* **2020**, *41* (3), 34.
(31) Soloveva, O. V.; Solovev, S. A.; Vankov, Y. V.; Shakurova, R. Z. Experimental Studies of the Effective Thermal Conductivity of Polyurethane Foams with Different Morphologies. *Processes* **2022**, *10* (11), 2257.
(32) Rochefort, M.; Ripley, L.; Holland, P.; Coppock, V. Phenolic Foam. U.S. Patent 9,896,559 B2, 2018.
(33) Rangari, V. K.; Hassan, T. A.; Zhou, Y.; Mahfuz, H.; Jeelani, S.; Prorok, B. C. Cloisite Clay-Infused Phenolic Foam Nanocomposites. *J. Appl. Polym. Sci.* **2007**, *103* (1), 308−314.
(34) Song, F.; Li, Z.; Jia, P.; Bo, C.; Zhang, M.; Hu, L.; Zhou, Y. Phosphorus-Containing Tung Oil-Based Siloxane Toughened Phenolic Foam with Good Mechanical Properties, Fire Performance and Low Thermal Conductivity. *Mater. Des.* **2020**, *192*, 108668.
(35) Xu, P.; Yu, Y.; Chang, M.; Chang, J. Preparation and Characterization of Bio-Oil Phenolic Foam Reinforced with Montmorillonite. *Polymers* **2019**, *11* (9), 1471.
(36) Guo, Y.; Hu, L.; Bo, C.; Shang, Q.; Feng, G.; Jia, P.; Zhang, B.; Zhou, Y. Mechanical Property of Lignin-Modified Phenolic Foam Enhanced by Nano-SiO_2 via a Novel Method. *Chem. Pap.* **2018**, *72* (3), 763−767.
(37) Coppock, V. Toughened Phenolic Foam. U.S. Patent 20,070,265,362 A1, 2007.

https://doi.org/10.1021/acsomega.3c07967
ACS Omega 2024, 9, 4695−4704